Highly penetrative, drug-loaded nanocarriers improve treatment of glioblastoma

Jiangbing Zhou[a,b,1], Toral R. Patel[b,1], Rachael W. Sirianni[c], Garth Strohbehn[a], Ming-Qiang Zheng[c], Nha Duong[a], Thomas Schafbauer[c], Anita J. Huttner[d], Yiyun Huang[c], Richard E. Carson[a,c], Ying Zhang[e], David J. Sullivan, Jr.[e], Joseph M. Piepmeier[b], and W. Mark Saltzman[a,2]

Departments of [a]Biomedical Engineering, [b]Neurosurgery, [c]Diagnostic Radiology, and [d]Pathology, Yale University, New Haven, CT 06511; and [e]W. Harry Feinstone Department of Molecular Microbiology and Immunology, Bloomberg School of Public Health, Johns Hopkins University, Baltimore, MD 21205

Edited* by Robert Langer, Massachusetts Institute of Technology, Cambridge, MA, and approved May 20, 2013 (received for review March 8, 2013)

Current therapy for glioblastoma multiforme is insufficient, with nearly universal recurrence. Available drug therapies are unsuccessful because they fail to penetrate through the region of the brain containing tumor cells and they fail to kill the cells most responsible for tumor development and therapy resistance, brain cancer stem cells (BCSCs). To address these challenges, we combined two major advances in technology: (*i*) brain-penetrating polymeric nanoparticles that can be loaded with drugs and are optimized for intracranial convection-enhanced delivery and (*ii*) repurposed compounds, previously used in Food and Drug Administration-approved products, which were identified through library screening to target BCSCs. Using fluorescence imaging and positron emission tomography, we demonstrate that brain-penetrating nanoparticles can be delivered to large intracranial volumes in both rats and pigs. We identified several agents (from Food and Drug Administration-approved products) that potently inhibit proliferation and self-renewal of BCSCs. When loaded into brain-penetrating nanoparticles and administered by convection-enhanced delivery, one of these agents, dithiazanine iodide, significantly increased survival in rats bearing BCSC-derived xenografts. This unique approach to controlled delivery in the brain should have a significant impact on treatment of glioblastoma multiforme and suggests previously undescribed routes for drug and gene delivery to treat other diseases of the central nervous system.

Of the ~40,000 people diagnosed with primary brain tumors in the United States each year, an estimated 15,000 have glioblastoma multiforme (GBM), a World Health Organization grade IV malignant glioma (1). Despite considerable research efforts, the prognosis for GBM remains poor: median survival with standard-of-care therapy (surgery, systemic chemotherapy with temozolomide, and radiation) is 14.6 mo (2) and 5-y survival is 9.8% (3), with the vast majority of GBMs recurring within 2 cm of the original tumor focus (4). Histopathologically, GBM is characterized by its infiltrative nature and cellular heterogeneity, leading to a number of challenges that must be overcome by any presumptive therapy.

The blood–brain barrier (BBB) is a major obstacle to treating GBM (5). It is estimated that over 98% of small-molecule drugs and ~100% of large-molecule drugs or genes do not cross the BBB (6). Delivery of chemotherapeutics to the brain can be potentially achieved by using nanocarriers engineered for receptor-mediated transport across the BBB (7, 8), but the percentage of i. v. administered particles that enter the brain is low. It is not yet clear whether sufficient quantities of drug can be delivered by systemically administered nanoparticles to make this a useful method for treating tumors in the human brain. An alternate approach is to bypass the BBB: Clinical trials have demonstrated that the BBB can be bypassed with direct, locoregional delivery of therapeutic agents. For example, local implantation of a drug-loaded biodegradable polymer wafer (presently marketed as Gliadel), which slowly releases carmustine over a prolonged period, is a safe method for treating GBM. However, use of the Gliadel wafer results in only modest improvements in patient survival, typically 2 mo (9, 10). In prior work we showed that these wafers produce high interstitial drug concentrations in the tissue near the implant, but—because drugs move from the implant into the tissue by diffusion—penetration into tissue is limited to ~1 mm, which could limit their efficacy (11, 12).

We hypothesize that treatment of GBM can be improved by attention to three challenges: (*i*) enhancing the depth of penetration of locally delivered therapeutic agents, (*ii*) providing for long-term release of active agents, and (*iii*) delivering agents that are known to be effective against the cells that are most important in tumor recurrence. The first challenge can be addressed by convection-enhanced delivery (CED), in which agents are infused into the brain under a positive pressure gradient, creating bulk fluid movement in the brain interstitium (13). Recent clinical trials show that CED is safe and feasible (14–16), but CED alone is not sufficient to improve GBM treatment. For example, CED of a targeted toxin in aqueous suspension failed to show survival advantages over Gliadel wafers (14, 17). Although CED of drugs in solution results in increased penetration, most drugs have short half-lives in the brain and, as a result, they disappear soon after the infusion stops (17, 18). Loading of agents into nanocarriers—such as liposomes, micelles, dendrimers, or nanoparticles—can protect them from clearance. Significant progress has been made in CED of liposomes to the brain (19), although it is not clear that liposomes offer the advantage of long-term release. By contrast, CED of polymeric nanoparticles, such as nanoparticles made of poly(lactide-coglycolide) (PLGA), offers the possibility of controlled agent release. However, CED of PLGA nanoparticles, which are typically 100–200 nm in diameter, has been limited by the failure of particles to move by convection through the brain interstitial spaces (20–23), which are 38–64 nm in normal brain (24) and 7–100 nm in regions with tumor (25). Therefore, to overcome the first and second challenges, it is necessary to synthesize polymer nanocarriers that are much smaller than conventional particles and still capable of efficient drug loading and controlled release. We report here reliable methods for making PLGA nanoparticles with these characteristics.

Drug developers have long been frustrated by the BBB, which severely limits the types of agents that can be tested for activity in the brain. We reasoned that creation of safe, versatile, brain-penetrating nanocarriers should enable direct testing of novel agents that address the complexity of GBM biology. For example, cells isolated from distinct regions of a given GBM bear grossly different expression signatures but seem to arise from a common

Author contributions: J.Z., T.R.P., R.W.S., R.E.C., J.M.P., and W.M.S. designed research; J.Z., T.R.P., R.W.S., G.S., M.-Q.Z., and T.S. performed research; Y.Z. and D.J.S. contributed new reagents/analytic tools; J.Z., T.R.P., R.W.S., G.S., M.-Q.Z., N.D., T.S., A.J.H., Y.H., R.E.C., Y.Z., D.J.S., J.M.P., and W.M.S. analyzed data; and J.Z., T.R.P., R.W.S., G.S., N.D., and W.M.S. wrote the paper.

The authors declare no conflict of interest.

*This Direct Submission article had a prearranged editor.

[1]J.Z. and T.R.P. contributed equally to this work.

[2]To whom correspondence should be addressed. E-mail: mark.saltzman@yale.edu.

This article contains supporting information online at www.pnas.org/lookup/suppl/doi:10.1073/pnas.1304504110/-/DCSupplemental.

progenitor (26): A small subpopulation of these progenitors drives tumor progression, promotes angiogenesis, and influences tumor cell migration (27–30). These cells have features of primitive neural stem cells and are called brain cancer stem cells (BCSCs) (29, 31–37). BCSCs, many of which are marked by CD133 (PROM1), are resistant to conventional drugs (28, 38), including carboplatin, cisplatin, paclitaxel, doxorubicin, vincristine, methotrexate, and temozolomide (39–42), as well as radiotherapy (29). These observations suggest that agents that affect BCSCs are more likely to lead to a cure for GBM (28, 38, 43, 44). Therefore, to illustrate the translational potential of brain-penetrating nanoparticles, we conducted a screen of ~2,000 compounds that were previously used in Food and Drug Administration (FDA)-approved products for their ability to inhibit patient-derived BCSCs, encapsulated the best agents to emerge from the screen into brain-penetrating PLGA nanoparticles, and administered these nanocarriers by CED in a BCSC-derived xenograft model of GBM.

Results

Synthesis of PLGA Nanoparticles. PLGA nanoparticles were synthesized using a single-emulsion, solvent evaporation technique. Dichloromethane (DCM) was chosen initially as the solvent owing to its ability to dissolve a wide range of hydrophobic drugs. To produce particles of the desired diameter, we developed a partial centrifugation technique. Specifically, after solvent evaporation and before particle washing, the particle solution was subjected to low-speed centrifugation (8,000 × *g* for 10 min), which caused larger particles to pellet while keeping the smaller particles in the supernatant. The initial pellet contained comparatively large nanoparticles and was removed (Fig. 1*A*). Nanoparticles in the supernatant were collected and washed using high-speed centrifugation (100,000 × *g* for 30 min). SEM showed that nanoparticles isolated using this protocol were 74 ± 18 nm in diameter and morphologically spherical (Fig. 1*B*). The typical yield for this fabrication was 12 ± 2%. In comparison, nanoparticles made using the same materials but with conventional centrifugation techniques were 150 ± 30 nm in diameter, with an average yield of 55 ± 5% (Fig. 1*C*). Organic solvents used for preparing polymer solution are known to affect the size of PLGA nanoparticles synthesized through emulsion procedures (45). In particular, partially water-miscible organic solvents—such as benzyl alcohol, butyl lactate, and ethyl acetate (EA)—allow nanoparticle formulation through an emulsion-diffusion mechanism and are able to produce smaller nanoparticles than water-immiscible solvents such as DCM (45). Therefore, we hypothesized that replacing DCM with partially water-miscible organic solvents could improve the yield of small nanoparticles. EA was chosen because of its low toxicity. Nanoparticles synthesized using EA as the solvent instead of DCM were 65 ± 16 nm in diameter and morphologically spherical. The yield was improved with EA: 44 ± 3% (Fig. 1*D*).

Cryoprotection to Prevent Aggregation of PLGA Nanoparticles. Lyophilization is a technique commonly used to stabilize nanoparticles for long-term storage. However, lyophilization can also cause nanoparticles to aggregate, making them difficult to resuspend in an aqueous solution. Furthermore, particle aggregation, if it did occur, could complicate CED infusion and restrict penetration in the brain. To reduce aggregation, we used the disaccharide trehalose as an excipient, which was added to the nanoparticle suspension at a ratio of 0.5:1 (trehalose:nanoparticles) by mass immediately before lyophilization (46, 47).

The addition of trehalose did not alter nanoparticle size, morphology, or yield. SEM images demonstrated that trehalose enhanced the separation of nanoparticles from one another (Fig. 1*E*) compared with nanoparticles lyophilized without trehalose (Fig. 1*D*). Reconstitution of cryoprotected nanoparticles resulted in a homogenous solution, whereas reconstitution of nanoparticles lyophilized without trehalose cryoprotection resulted in sedimentation over time, which caused clogging of the CED device and prevented infusion at a consistent pressure. We also determined hydrodynamic diameters of nanoparticles in PBS solution by Zetasizer (Malvern) and observed a similar trend in size change when the modifications described above were applied (Table S1).

CED of PLGA Nanoparticles in the Rat Brain. We next sought to assess the effects of particle size and cryoprotection on intracranial CED and volume of distribution (V_d). We synthesized both small PLGA nanoparticles and standard PLGA nanoparticles. Before lyophilization, nanoparticles from each group were further divided into two groups: with or without trehalose cryoprotection. Nanoparticles were loaded with coumarin-6 (C6), a fluorescent dye commonly used for visualization. Small and standard nanoparticles had mean diameters of 71 nm ± 13 nm and 147 nm ± 27 nm, respectively. Consistent with previous work (48), release of C6 from nanoparticles was negligible (<0.5%) at 72 h.

Sixteen nude rats received 20-μL infusions (V_i) of C6-loaded nanoparticles into the right striatum via CED ($n = 4$ per group). Animals were killed 30 min after infusion and their brains were sectioned and analyzed using fluorescence microscopy to determine V_d. Both small size and trehalose cryoprotection independently contributed to increased penetrance of nanoparticles in brain parenchyma, and small nanoparticles with cryoprotectant resulted in the best distribution in the brain (Fig. 2). We call the small, trehalose-treated carriers brain-penetrating nanoparticles, because of this enhanced ability to distribute in the brain via CED. Mean V_d for brain-penetrating particles was 74 ± 7 mm^3 (V_d/V_i = 3.7 ± 0.3), whereas mean V_d for standard particles without trehalose was 11 ± 3 mm^3 (V_d/V_i = 0.6 ± 0.1). Subgroup analyses demonstrate that both small size and coating with trehalose independently improve V_d ($P < 0.05$). Interestingly, for brain-penetrating nanoparticles compared with standard nanoparticles, the V_d/V_i increased toward the theoretical limit of 5, which is usually only achievable by ideal free drugs in solution (23, 49–51).

Live, Noninvasive Imaging of Brain-Penetrating Nanoparticles in the Rat Brain Using PET. The clinical translation of delivery systems for the treatment of intracranial diseases has been hindered by an

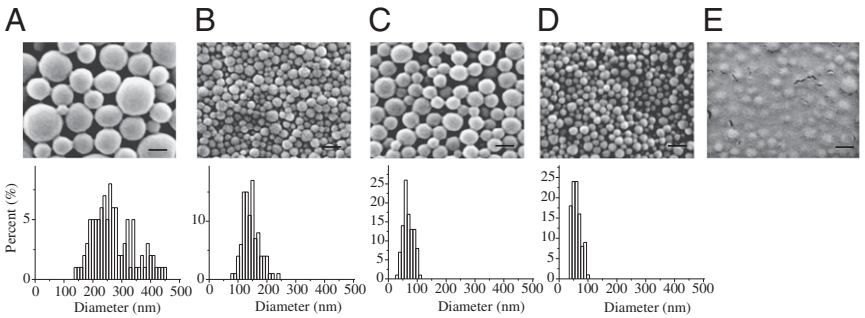

Fig. 1. Characterization of nanoparticles. Morphology and size distribution of PLGA nanoparticles obtained using DCM in (*A*) the pellet from the first low-speed centrifugation, (*B*) the pellet from the high-speed centrifugation of the supernatant from the first centrifugation (small nanoparticles), and (*C*) nanoparticles synthesized using standard procedures. (*D*) Morphology and size distribution of small nanoparticles with EA used as solvent. (*E*) SEM of small nanoparticles cryoprotected with trehalose. (Scale bars, 200 nm.) By using a partial centrifugation technique, a homogenous population of small nanoparticles was isolated.

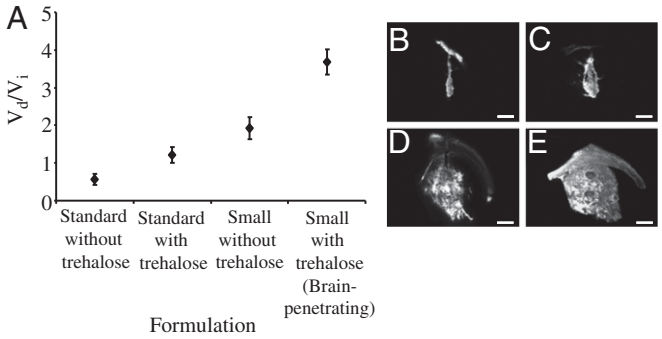

Fig. 2. Penetration of nanoparticles delivered by CED in the rat brain. (*A*) V_d/V_i for C6-loaded nanoparticles of the indicated formulations. Fluorescence microscopy images of rat striatum (coronal sections) after CED administration of standard or small nanoparticles: (*B*) standard without trehalose, (*C*) standard with trehalose, (*D*) small without trehalose, and (*E*) small with trehalose (brain-penetrating). Statistical analyses demonstrate that both small size and coating with trehalose independently improves V_d ($P < 0.05$). (Scale bars, 1 mm.)

inability to noninvasively characterize in vivo distribution. We applied a modular radiolabeling strategy to permit noninvasive, quantitative PET imaging of our brain-penetrating nanoparticles (52). PLGA nanoparticles were modified to display surface-bound palmitylated avidin, which enabled easy radiolabeling of nanoparticles with *N*-(4-[^{18}F]fluorobenzyl)propanamido-PEG$_4$-Biotin ([^{18}F]NPB4), a biotinylated, gamma-emitting compound that can be detected with PET (53, 54). [^{18}F]NPB4-labeled and C6-loaded PLGA nanoparticles were synthesized and delivered via CED to the right striatum of five Sprague Dawley rats. Three rats received infusions of brain-penetrating PLGA nanoparticles, and the other two rats received infusions of standard nanoparticles without trehalose ($V_i = 20$ μL for both groups) (Fig. 3*A*). When measured noninvasively and quantitatively with PET imaging, the mean V_d for the brain-penetrating nanoparticles was 111 ± 3 mm^3 ($V_d/V_i = 5.5 \pm 0.2$), whereas the mean V_d for the standard nanoparticles was 53 ± 23 mm^3 ($V_d/V_i = 2.6 \pm 1.2$) (Fig. 3*B*). Postmortem analysis using fluorescence microscopy revealed that the mean V_d for the brain-penetrating nanoparticles was 82 mm^3 ± 5 mm^3 ($V_d/V_i = 4.1 \pm 0.2$), whereas the mean V_d for the standard nanoparticles was 11 mm^3 ± 4 mm^3 ($V_d/V_i = 0.5 \pm 0.2$) (Fig. 3*C*). The V_d/V_i determined for these brain-penetrating nanoparticles by fluorescence analysis (4.1 ± 0.2) was similar to the V_d/V_i obtained in particles without [^{18}F]NPB4 coatings (3.7 ± 0.3; see above), suggesting that our method for ^{18}F labeling does not hinder particle penetration. Thus, consistent with imaging results from destructive fluorescence microscopy of brain sections, quantitative analysis of noninvasive PET imaging demonstrated that brain-penetrating nanoparticles reached a larger volume of spatial distribution than standard nanoparticles (Fig. 3*D*). We note that the differences between distribution volumes calculated from PET images and fluorescence images are likely due to the substantial differences in sensitivity and spatial resolution for these two imaging techniques.

CED of Brain-Penetrating Nanoparticles in the Pig Brain. Rodent brains are much smaller than human brains, so it is difficult to assess whether the V_d obtained after CED in the rat is relevant to treatment of human disease. To extend our analysis to larger brains, we infused brain-penetrating, C6-loaded PLGA nanoparticles into the striatum of pig brains ($n = 4$) using our CED technique ($V_i = 338$ μL). Animals were killed 120 min postinfusion and their brains were analyzed with fluorescence microscopy to determine V_d (Fig. 4). Brain-penetrating PLGA nanoparticles delivered by CED penetrated pig brain tissue with a mean V_d of 1,180 mm^3 ± 37 mm^3, which resulted in $V_d/V_i = 3.5 \pm 0.1$, similar to the value obtained in the rat (again, much closer to the theoretical limit of 5 than previously achieved with similar nanoparticles). The extent of nanoparticle penetration in the pig brain was >1 cm (Fig. 4). Our brain-penetrating nanoparticles distribute to volumes that are clinically relevant, because the vast majority of GBMs recur within 2 cm of their original location (4). Even greater penetration is possible in humans, because infusion volumes of up to 72 mL have been used safely in previous clinical trials (14).

Delivery of Chemotherapy for Solid Brain Tumor. We next sought to assess whether these brain-penetrating PLGA nanoparticles could be used to treat intracranial tumors. For initial studies, we created intracranial tumors in immunocompromised rats by injection of U87MG, the most commonly used human GBM cell line, and we treated the animals with CED of paclitaxel, a drug previously shown to inhibit proliferation of U87MG. Our results showed that paclitaxel was efficiently encapsulated into brain-penetrating nanoparticles, and CED of paclitaxel-loaded brain-penetrating nanoparticles enhanced survival in tumor-bearing rats: Median survival times for rats receiving brain-penetrating, paclitaxel-loaded particles were significantly longer than for rats receiving either free paclitaxel or standard, paclitaxel-loaded nanoparticles (*SI Text* and Fig. S1).

We are aware that a histopathologic hallmark of GBM is its infiltrative nature. The U87MG cell line has been propagated in cell culture for many years and has lost its infiltrative nature in vivo. After intracranial injection, U87MG cells form solid tumors that are histopathologically distinct from human GBM (55) (Fig. S2*A*). In contrast, several recent studies have demonstrated that a murine xenograft model using human BCSCs has the ability to recapitulate human GBM histopathology (37, 56). To test whether BCSCs were able to form such tumors in nude rats, we inoculated GS5, a well-characterized BCSC line (37, 57) in rat brains. Consistent with the findings in mouse brains (37, 57), GS5 tumors in the brain of nude rats are highly infiltrative and histopathologically similar to human GBM (Fig. S2 *B* and *C*). Therefore, we sought to improve the translational relevance of our studies by (*i*) identifying agents that are effective against patient-derived BCSCs and (*ii*) delivering these agents in an animal model that is reflective of human GBM.

We screened a library of ~2,000 compounds that have been used by humans, in FDA-approved products, against GS5 for growth-inhibitory activity (Fig. 5*A*) (58, 59). Briefly, GS5 cells were plated in 96-well format, treated with 5 μM drug, and evaluated for viability 3 d later using the thiazolyl blue tetrazolium bromide (MTT) assay. Initial hits were subsequently evaluated for inhibition of GS5 sphere formation, a measure of BCSC self-renewal. Thirty-two candidate compounds were identified (Table

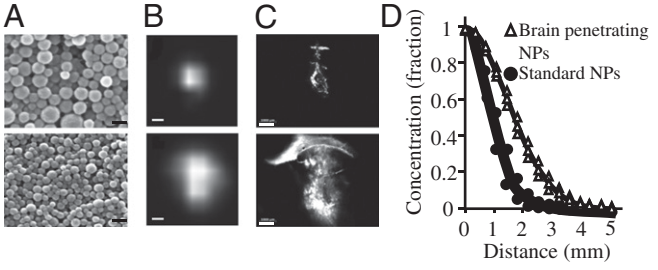

Fig. 3. PET imaging of nanoparticles delivered via CED in the brain. (*A*) Morphology of standard (*Upper*) and small (*Lower*) nanoparticles loaded with C6 and labeled with [^{18}F]NPB4. (Scale bar, 200 nm.) (*B*) Representative PET images of [^{18}F]NPB4-labeled and C6-loaded nanoparticles in the brain, acquired in a 1-h scan. (*C*) Corresponding fluorescence microscopy images (coronal sections). (Scale bars, 1 mm.) (*D*) Radial concentration profiles of nanoparticles as determined by PET imaging (△, brain-penetrating nanoparticles; ●, standard nanoparticles). Noninvasive PET imaging confirms the distribution data obtained via destructive fluorescence microscopy.

ENGINEERING

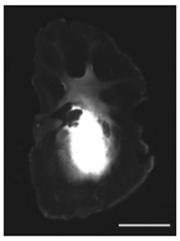

Fig. 4. Distribution of brain-penetrating nanoparticles in the pig brain. Representative fluorescence microscopy image (coronal section) demonstrates wide particle distribution throughout the striatum. (Scale bar, 1 cm.)

S2), some of which were later confirmed in an independent high-throughput screen in BCSCs (60). The BCSC growth-inhibiting activity of many compounds was confirmed using AlamarBlue. One compound in particular, the anti-helminthic cyanine dye dithiazanine iodide (DI), potently inhibited GS5 proliferation, with an IC_{50} of 79 nM. Treatment with DI inhibited GS5 sphere formation, a measure of BCSC self-renewal, by 94%. DI-mediated inhibition of BCSC sphere formation was further confirmed by a limiting dilution assay with pretreatment of DI (Fig. S3). Additionally, DI decreased the CD133+ cell population by 57% (Fig. 5*B*). DI was evaluated in two additional BCSC lines isolated in our laboratory, PS11 and PS16, and showed similar anti-BCSC effects (Fig. 5*B* and Fig. S3).

We next evaluated whether CED of brain-penetrating, DI-loaded nanoparticles could prevent tumor growth in our histopathologically relevant model of GBM. DI was loaded into brain-penetrating nanoparticles with encapsulation efficiency of 19% and yield of 18%. Brain-penetrating, DI-loaded nanoparticles were spherical and had an average diameter of 70 ± 19 nm (Fig. 6 *A* and *B*). DI was released from brain-penetrating nanoparticles in a controlled manner over several weeks (Fig. 6*C*). To evaluate their efficacy in vivo, brain-penetrating, DI-loaded nanoparticles were administrated via a single infusion into rat brains bearing GS5-derived tumors. Brain-penetrating DI nanoparticles significantly increased the median survival of tumor-bearing rats (Fig. 6*D*). Kaplan–Meier analysis revealed that rats treated with brain-penetrating, DI-loaded nanoparticles had significant improvements in median survival, which was over 280 d. By contrast, rats receiving standard nanoparticles, free drug, blank/unloaded nanoparticles, and no treatment had a median survival of 180, 177, 156, and 147 d, respectively ($P < 0.005$ for each comparison) (Fig. 6*D*). We also note that in our experience to date, 48 control animals (i.e., animals receiving GS5-derived tumors but no treatment) all died of histologically confirmed tumors within 200 d of tumor initiation, suggesting that the probability of tumor initiation using our procedures is near 100%.

We also tested two other compounds that exhibited activity in our in vitro screening experiments. Both anisomycin and digoxin performed well on in vitro assays against BCSCs and were loaded efficiently into brain-penetrating nanoparticles that provided controlled release. In pilot experiments, however, CED delivery of anisomycin-loaded or digoxin-loaded particles provided no survival benefit to rats with intracranial BCSC-derived tumors (Figs. S4 and S5).

Discussion

In this report, we describe a unique strategy for the treatment of GBM that addresses the two most important obstacles to effective therapy: (*i*) the infiltrative nature of GBM and (*ii*) the genetic heterogeneity of the tumor and chemoresistance of BCSCs, which give rise to drug delivery and discovery challenges, respectively. To overcome the challenges associated with drug delivery, we developed a controlled-release delivery system composed of brain-penetrating PLGA nanoparticles that can penetrate to substantially (approximately sevenfold) higher volumes than conventional PLGA nanoparticles when delivered intracranially using CED. The penetration of these particles is as good as any previously reported nanoparticle systems: For example, the V_d/V_i achieved in our studies is comparable to those achieved with nanoliposomal delivery systems in rats (61). PLGA particles have many advantages over liposomal formulations including lower toxicity and control of drug release. Further, we showed that the brain-penetrating ability of these particles extends to large animals: PLGA nanoparticles delivered in pig brains using CED penetrated to volumes of ~1,180 mm^3. Because the vast majority of GBMs recur within 2 cm of the original tumor focus (4), the penetrative capacity of these brain-penetrating nanoparticles when delivered by CED can address the infiltrative nature of GBM. We also surface-modified nanoparticles with [^{18}F]NPB4 using streptavidin–biotin conjugation, which allowed us to track the nanoparticles during the CED procedure using noninvasive PET imaging. This capability will allow clinicians to visualize nanoparticles delivered by CED and ensure distribution of the therapeutic agent throughout the brain regions most likely in need of treatment.

In comparison with currently available nanocarrier drug delivery systems, this platform has at least three clear advantages. First, the polymer has an excellent safety profile: PLGA was part of an FDA-approved formulation in 1969 and has been safely used in clinical practice since that time. Specifically, PLGA is commonly used in suture material and is a component of several controlled-release drug delivery products. Second, the release kinetics of PLGA nanoparticles can be more easily modulated than those of competing nanocarrier systems used in intracranial applications, namely liposomes and micelles. Third, the versatile surface modification approach described in this study enables rapid, modular attachment of biotinylated agents, thereby allowing for efficient labeling of nanoparticles with a host of cell-targeting and -penetrating agents. Finally, the exceptionally small diameters allow these nanoparticles to penetrate relatively large, clinically relevant volumes when delivered by CED. In short, this is a versatile delivery platform for the central nervous system, which we have optimized for translational medicine.

This delivery platform allows for the direct testing of new agents for treating GBM. BCSC resistance to conventional chemotherapeutics is a major challenge in GBM. We used a library screening approach to identify agents that have improved activity against BCSCs. Of the 1,937 compounds we screened, we settled on DI for initial testing owing to its abilities to inhibit growth, inhibit self-renewal, and encourage differentiation of cells it fails to kill. We note that recent reports by other groups confirm many of the other potential drugs we identified, such as emetine (60). Brain-penetrating, DI-loaded PLGA nanoparticles inhibit growth of intracranial tumors in an animal model that closely reflects many aspects of human GBM. We demonstrated the effectiveness

A

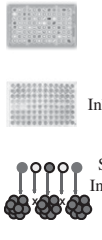

B

Test	GS5	PS11	PS16
IC50	79 nM	233 nM	62 nM
NS Inhibition (%Control)	93.6 ± 5.5%	91.2 ± 8.2%	99.7 ± 17.5%
CD133+ (%Control) **	56.6 ± 12.7%	58.7 ± 18.6%	18.2 ± 6.6%

Fig. 5. Anti-BCSC activity of DI. (*A*) Schematic of small-molecule compound screening using MTT and self-renewal assays. (*B*) Inhibition of DI on BCSC cell proliferation, sphere formation and CD133+ fraction in culture. NS, neurosphere.

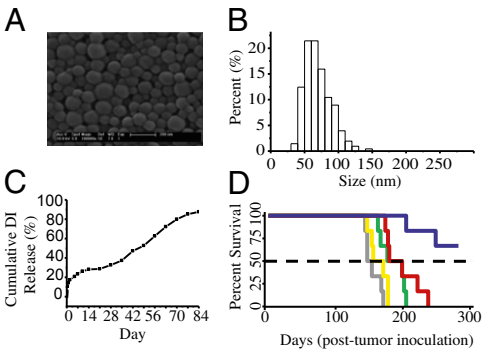

Fig. 6. Synthesis and antitumor effects of nanoparticle-encapsulated DI on BCSC xenograft tumors in the rat. (*A*) Morphology, (*B*) size distribution, and (*C*) controlled-release profile of small DI-loaded nanoparticles (NPs). (*D*) Kaplan–Meier survival curves for tumor-bearing rats with indicated treatments: blue line, brain-penetrating DI NPs (median survival >280 d); red line, standard DI NPs (median survival 180 d); green line, free DI (median survival 177 d); yellow line, blank NPs (median survival 156 d); gray line, no treatment (median survival 147 d). Rats treated with brain-penetrating, DI-loaded NPs had significant improvements in median survival compared with all other groups ($P < 0.005$ for each comparison). The experiment shown in *D* has been repeated, on separate occasions, with similar results (one of the replicates is shown in Fig. S6).

of our approach on intracranial tumors that were initiated in the striatum, which is the most common experimental site. Although this is not the most common location for occurrence of human GBM, which is a disease of the white matter, the striatum is the largest, most homogenous area available in the rodent brain and is thus the best location for evaluating the effectiveness of CED. In addition, our experimental results in the rodent and pig demonstrate that the CED-delivered nanoparticles are able to travel through white matter tracts and across the corpus callosum, which enhances their clinical relevance. More broadly, our work suggests that improved treatment of GBM might be achievable if obstacles pertaining to both the infiltrative and chemoresistant properties of the disease can be sufficiently overcome.

We have tested our platform with two other drugs that seemed highly active against BCSCs in our screen: digoxin and anisomycin. Interestingly, efficacy in vivo—as determined by increase in median survival after a single treatment by CED with drug-loaded, brain-penetrating nanoparticles—was not predictable from its potency in cell culture. For example, the cardiac glycoside digoxin and the antibiotic anisomycin exhibited IC_{50} values against BCSCs comparable to DI. Although these drugs were loaded efficiently into brain-penetrating nanoparticles, and administered without problem to rats with intracranial tumors, the survival benefits were modest compared with DI. Further work may reveal conditions that lead to prolonged survival with CED of brain-penetrating nanoparticles loaded with digoxin or anisomycin—by refinements in V_d, nanoparticle design, or dosing scheme—but these results highlight the striking effectiveness of DI-loaded, brain-penetrating nanoparticles when administered by CED. The observation that DI is more effective in vivo than other drugs with comparable in vitro activity also suggests that it will be important to evaluate the effectiveness of these agents in intracranial tumors formed from BCSC representing different subgroups in The Cancer Genome Atlas (62)—which likely differ in vascularity, BBB integrity, and other factors—to identify the relationship between tumor biology, agent activity, and distribution of nanoparticles in the complex cellular milieu of brain tumors.

Although brain-penetrating PLGA nanoparticles were evaluated here against intracranial tumors with small molecule drugs, the system can be tailored for application to a host of CNS diseases. For example, surface modification or size fractionation could produce particles well suited for the treatment of certain neurodegenerative disorders, such as Parkinson disease or Huntington disease, as well as diseases with localized cerebral dysfunction, such as stroke. These particles also have the potential to encapsulate not only hydrophobic drugs but also a variety of nucleic acids for gene therapy applications (63). The particles are simple in composition, which should aid in clinical translation. A recent study reported by Hanes and coworkers (64) suggests that a dense PEG coating is needed to allow nanoparticles as large as 114 nm in diameter to diffuse passively in the brain: Without the PEG coating, transport of particles of this size was strongly hindered. Our results suggest that PEG is not needed for unhindered transport of smaller particles (~70 nm) during CED. Owing to their ability to penetrate brain tissue, their construction from safe components, and their ability to control agent release, we anticipate that this brain-penetrating PLGA nanoparticle delivery platform will have significant clinical impact.

Methods

Nanoparticle Synthesis. Nanoparticles loaded with C6 or paclitaxel were synthesized by a single-emulsion solvent evaporation technique. One hundred milligrams of PLGA (50:50; Polysciences and Birmingham) and agents to be encapsulated were dissolved in 2 mL DCM or EA. The polymer/drug solution was then added dropwise to 4 mL of 2.5% polyvinyl alcohol (PVA) as the outer aqueous phase and sonicated to form an emulsion. The emulsion was poured into a beaker containing aqueous 0.3% (vol/vol) PVA and stirred at room temperature for 3 h (DCM as solvent) or 5 h (EA as solvent) to allow the solvent to evaporate and particles to harden.

To synthesize standard nanoparticles, following the solvent evaporation phase, the nanoparticle solution was subjected to typical centrifugation speeds (11,500 × *g* for 15 min, three times) and the pellet was collected. To synthesize small nanoparticles, following the solvent evaporation phase, the nanoparticle solution was first centrifuged at low speed (8,000 × *g* for 10 min) to pellet the large particles. The supernatant was decanted and small nanoparticles were collected through high-speed ultracentrifugation (100,000 × *g* for 30 min, two times).

To prevent nanoparticle aggregation during lyophilization, trehalose was added to the final aqueous solution at a ratio of 0.5:1 (trehalose:nanoparticles) by mass immediately before lyophilization.

Drug Screening. Drug screening was performed in clear 96-well plates using a compound library that contains 1,937 compounds that are or were components of an FDA-approved product (58, 59). The procedure for screening is depicted in Fig. 5*A*. Cell proliferation and sphere formation assays were performed as described below.

Antitumor Activity in Xenograft Model. To establish tumors for evaluation of paclitaxel-loaded PLGA nanoparticles, nude rats were first anesthetized with a ketamine/xylazine mixture ($n = 5$ per control group, $n = 10$ per treatment group). Animals were then prepped with betadine and alcohol and placed in a stereotactic frame. A linear midline incision was made and a 1.5-mm-diameter hole was drilled in the skull 3 mm lateral and 0.5 mm anterior to bregma. The right striatum was targeted. A 26G Hamilton syringe was inserted to a depth of 5 mm. The tissue was allowed to equilibrate mechanically for 5 min. Subsequently, 5×10^5 U87MG cells in 2 μL of PBS was injected into the brain at a rate of 0.5 μL/min. The burr hole was filled with bone wax (Lukens), the scalp was closed with surgical staples, and the rat was removed to a clean cage with free access to food and water mixed with ibuprofen. Seven days after tumor inoculation, all rats received a single treatment as indicated. Rats were again anesthetized, prepped, and placed in a stereotactic frame. The wound was reopened and the Hamilton syringe was oriented as described previously. Twenty microliters of either nanoparticles (100 mg/mL) or equivalent free drug were infused continuously at a rate of 0.667μL/min. Following infusion, the syringe was left in place for 5 min, after which it was removed. The burr hole was filled with bone wax (Lukens), the scalp was closed with surgical staples, and the rat was removed to a clean cage with free access to food and water mixed with ibuprofen. The animals' weight, grooming, and general health were monitored on a daily basis. Animals were killed after either a 15% loss in body weight or when it was humanely necessary owing to clinical symptoms. The same procedures were used to evaluate DI nanoparticles, except that GS5 cells were used and a single treatment with 6-mg nanoparticles was performed 10 d after tumor inoculation, as indicated ($n = 6$ per group).

Statistical Analysis. All data were collected in triplicate, unless otherwise noted, and reported as means and SD. Comparison of two conditions was evaluated by a paired Student *t* test. Kaplan–Meier analysis was used to evaluate the effect of various treatments on survival. A $P \leq 0.05$ was considered to indicate a statistically significant difference.

More information is given in *SI Text*.

ACKNOWLEDGMENTS. We thank Whitney Sheen for technical assistance and Jie Liu for providing a histological image of U87 intracranial tumors. This work was supported by National Institutes of Health Grant CA149128, the Chicago Institute of Neurosurgery and Neuroresearch Foundation, the Voices Against Brain Cancer Foundation, the B*Cured Foundation, and a pilot grant from the Yale Institute for Nanoscience and Quantum Engineering.

1. Mrugala MM, Chamberlain MC (2008) Mechanisms of disease: Temozolomide and glioblastoma—look to the future. *Nat Clin Pract Oncol* 5(8):476–486.
2. Stupp R, et al.; European Organisation for Research and Treatment of Cancer Brain Tumor and Radiotherapy Groups; National Cancer Institute of Canada Clinical Trials Group (2005) Radiotherapy plus concomitant and adjuvant temozolomide for glioblastoma. *N Engl J Med* 352(10):987–996.
3. Stupp R, et al.; European Organisation for Research and Treatment of Cancer Brain Tumour and Radiation Oncology Groups; National Cancer Institute of Canada Clinical Trials Group (2009) Effects of radiotherapy with concomitant and adjuvant temozolomide versus radiotherapy alone on survival in glioblastoma in a randomised phase III study: 5-year analysis of the EORTC-NCIC trial. *Lancet Oncol* 10(5):459–466.
4. Hochberg FH, Pruitt A (1980) Assumptions in the radiotherapy of glioblastoma. *Neurology* 30(9):907–911.
5. Kreuter J (2001) Nanoparticulate systems for brain delivery of drugs. *Adv Drug Deliv Rev* 47(1):65–81.
6. Pardridge WM (2005) The blood-brain barrier and neurotherapeutics. *NeuroRx: The journal of the American Society for Experimental NeuroTherapeutics* 2(1):1–2.
7. Schneider T, et al. (2008) Brain tumor therapy by combined vaccination and antisense oligonucleotide delivery with nanoparticles. *J Neuroimmunol* 195(1-2):21–27.
8. Wohlfart S, et al. (2011) Treatment of glioblastoma with poly(isohexyl cyanoacrylate) nanoparticles. *Int J Pharm* 415(1-2):244–251.
9. Brem H, et al. (1991) Interstitial chemotherapy with drug polymer implants for the treatment of recurrent gliomas. *J Neurosurg* 74(3):441–446.
10. Brem H, et al.; The Polymer-brain Tumor Treatment Group (1995) Placebo-controlled trial of safety and efficacy of intraoperative controlled delivery by biodegradable polymers of chemotherapy for recurrent gliomas. *Lancet* 345(8956):1008–1012.
11. Fung LK, Shin M, Tyler B, Brem H, Saltzman WM (1996) Chemotherapeutic drugs released from polymers: distribution of 1,3-bis(2-chloroethyl)-1-nitrosourea in the rat brain. *Pharm Res* 13(5):671–682.
12. Fung LK, et al. (1998) Pharmacokinetics of interstitial delivery of carmustine, 4-hydroperoxycyclophosphamide, and paclitaxel from a biodegradable polymer implant in the monkey brain. *Cancer Res* 58(4):672–684.
13. Bobo RH, et al. (1994) Convection-enhanced delivery of macromolecules in the brain. *Proc Natl Acad Sci USA* 91(6):2076–2080.
14. Kunwar S, et al.; PRECISE Study Group (2010) Phase III randomized trial of CED of IL13-PE38QQR vs Gliadel wafers for recurrent glioblastoma. *Neuro-oncol* 12(8):871–881.
15. Sampson JH, et al. (2008) Intracerebral infusion of an EGFR-targeted toxin in recurrent malignant brain tumors. *Neuro-oncol* 10(3):320–329.
16. Jacobs A, et al. (2001) Positron-emission tomography of vector-mediated gene expression in gene therapy for gliomas. *Lancet* 358(9283):727–729.
17. Sampson JH, et al.; PRECISE Trial Investigators (2010) Poor drug distribution as a possible explanation for the results of the PRECISE trial. *J Neurosurg* 113(2):301–309.
18. Allard E, Passirani C, Benoit JP (2009) Convection-enhanced delivery of nanocarriers for the treatment of brain tumors. *Biomaterials* 30(12):2302–2318.
19. Krauze MT, et al. (2007) Convection-enhanced delivery of nanoliposomal CPT-11 (irinotecan) and PEGylated liposomal doxorubicin (Doxil) in rodent intracranial brain tumor xenografts. *Neuro-oncol* 9(4):393–403.
20. Sawyer AJ, Piepmeier JM, Saltzman WM (2006) New methods for direct delivery of chemotherapy for treating brain tumors. *Yale J Biol Med* 79(3-4):141–152.
21. Sawyer AJ, et al. (2011) Convection-enhanced delivery of camptothecin-loaded polymer nanoparticles for treatment of intracranial tumors. *Drug Deliv Transl Res* 1(1):34–42.
22. Neeves KB, Sawyer AJ, Foley CP, Saltzman WM, Olbricht WL (2007) Dilation and degradation of the brain extracellular matrix enhances penetration of infused polymer nanoparticles. *Brain Res* 1180:121–132.
23. Chen MY, et al. (2005) Surface properties, more than size, limiting convective distribution of virus-sized particles and viruses in the central nervous system. *J Neurosurg* 103(2):311–319.
24. Thorne RG, Nicholson C (2006) In vivo diffusion analysis with quantum dots and dextrans predicts the width of brain extracellular space. *Proc Natl Acad Sci USA* 103(14):5567–5572.
25. Hobbs SK, et al. (1998) Regulation of transport pathways in tumor vessels: Role of tumor type and microenvironment. *Proc Natl Acad Sci USA* 95(8):4607–4612.
26. Snuderl M, et al. (2011) Mosaic amplification of multiple receptor tyrosine kinase genes in glioblastoma. *Cancer Cell* 20(6):810–817.
27. Fan X, Salford LG, Widegren B (2007) Glioma stem cells: Evidence and limitation. *Semin Cancer Biol* 17(3):214–218.
28. Clarke MF (2004) Neurobiology: At the root of brain cancer. *Nature* 432(7015):281–282.
29. Bao S, et al. (2006) Glioma stem cells promote radioresistance by preferential activation of the DNA damage response. *Nature* 444(7120):756–760.
30. Calabrese C, et al. (2007) A perivascular niche for brain tumor stem cells. *Cancer Cell* 11(1):69–82.
31. Singh SK, et al. (2003) Identification of a cancer stem cell in human brain tumors. *Cancer Res* 63(18):5821–5828.
32. Galli R, et al. (2004) Isolation and characterization of tumorigenic, stem-like neural precursors from human glioblastoma. *Cancer Res* 64(19):7011–7021.
33. Singh SK, et al. (2004) Identification of human brain tumour initiating cells. *Nature* 432(7015):396–401.
34. Yuan X, et al. (2004) Isolation of cancer stem cells from adult glioblastoma multiforme. *Oncogene* 23(58):9392–9400.
35. Bao S, et al. (2006) Stem cell-like glioma cells promote tumor angiogenesis through vascular endothelial growth factor. *Cancer Res* 66(16):7843–7848.
36. Beier D, et al. (2007) CD133(+) and CD133(-) glioblastoma-derived cancer stem cells show differential growth characteristics and molecular profiles. *Cancer Res* 67(9):4010–4015.
37. Gunther HS, et al. (2008) Glioblastoma-derived stem cell-enriched cultures form distinct subgroups according to molecular and phenotypic criteria. *Oncogene* 27(20):2897–2909.
38. Jones RJ, Matsui WH, Smith BD (2004) Cancer stem cells: Are we missing the target? *J Natl Cancer Inst* 96(8):583–585.
39. Tang C, Chua CL, Ang BT (2007) Insights into the cancer stem cell model of glioma tumorigenesis. *Ann Acad Med Singapore* 36(5):352–357.
40. Liu G, et al. (2006) Analysis of gene expression and chemoresistance of CD133+ cancer stem cells in glioblastoma. *Mol Cancer* 5:67.
41. Eramo A, et al. (2006) Chemotherapy resistance of glioblastoma stem cells. *Cell Death Differ* 13(7):1238–1241.
42. Hirschmann-Jax C, et al. (2004) A distinct "side population" of cells with high drug efflux capacity in human tumor cells. *Proc Natl Acad Sci USA* 101(39):14228–14233.
43. Abbott A (2006) Cancer: The root of the problem. *Nature* 442(7104):742–743.
44. Reya T, Morrison SJ, Clarke MF, Weissman IL (2001) Stem cells, cancer, and cancer stem cells. *Nature* 414(6859):105–111.
45. Kocbek P, Baumgartner S, Kristl J (2006) Preparation and evaluation of nanosuspensions for enhancing the dissolution of poorly soluble drugs. *Int J Pharm* 312(1-2):179–186.
46. Anhorn MG, Mahler HC, Langer K (2008) Freeze drying of human serum albumin (HSA) nanoparticles with different excipients. *Int J Pharm* 363(1-2):162–169.
47. Konan YN, Gurny R, Allémann E (2002) Preparation and characterization of sterile and freeze-dried sub-200 nm nanoparticles. *Int J Pharm* 233(1-2):239–252.
48. Corrigan OI, Li X (2009) Quantifying drug release from PLGA nanoparticulates. *Eur J Pharm Sci* 37(3-4):477–485.
49. Levin VA, Fenstermacher JD, Patlak CS (1970) Sucrose and inulin space measurements of cerebral cortex in four mammalian species. *Am J Physiol* 219(5):1528–1533.
50. Nicholson C, Syková E (1998) Extracellular space structure revealed by diffusion analysis. *Trends Neurosci* 21(5):207–215.
51. Syková E, Nicholson C (2008) Diffusion in brain extracellular space. *Physiol Rev* 88(4):1277–1340.
52. Sirianni RW, Zheng MQ, Huang Y, Saltzman WM, Carson RE (2010) Development of dPET, a non-invasive imaging technique to measure the distribution of drugs after direct delivery to the brain. *J Nucl Med* 51(Suppl 1):829.
53. Fahmy TM, Samstein RM, Harness CC, Mark Saltzman W (2005) Surface modification of biodegradable polyesters with fatty acid conjugates for improved drug targeting. *Biomaterials* 26(28):5727–5736.
54. Zheng MQ, et al. (2011) PEG-Biotin labeled nanoparticles for tracking drug delivery and tumor therapy. *J Nucl Med* 52(Suppl 1):417.
55. Wong K, et al. (2011) Characterization of a human tumorsphere glioma orthotopic model using magnetic resonance imaging. *J Neurooncol* 104(2):473–481.
56. Lee J, et al. (2006) Tumor stem cells derived from glioblastomas cultured in bFGF and EGF more closely mirror the phenotype and genotype of primary tumors than do serum-cultured cell lines. *Cancer Cell* 9(5):391–403.
57. Wolpert F, et al. (2012) HLA-E contributes to an immune-inhibitory phenotype of glioblastoma stem-like cells. *J Neuroimmunol* 250(1-2):27–34.
58. Chong CR, Chen X, Shi L, Liu JO, Sullivan DJ, Jr. (2006) A clinical drug library screen identifies astemizole as an antimalarial agent. *Nat Chem Biol* 2(8):415–416.
59. Zhou J, et al. (2009) Cancer stem/progenitor cell active compound 8-quinolinol in combination with paclitaxel achieves an improved cure of breast cancer in the mouse model. *Breast Cancer Res Treat* 115(2):269–277.
60. Visnyei K, et al. (2011) A molecular screening approach to identify and characterize inhibitors of glioblastoma stem cells. *Mol Cancer Ther* 10(10):1818–1828.
61. Saito R, et al. (2006) Tissue affinity of the infusate affects the distribution volume during convection-enhanced delivery into rodent brains: Implications for local drug delivery. *J Neurosci Methods* 154(1-2):225–232.
62. Verhaak RG, et al.; Cancer Genome Atlas Research Network (2010) Integrated genomic analysis identifies clinically relevant subtypes of glioblastoma characterized by abnormalities in PDGFRA, IDH1, EGFR, and NF1. *Cancer Cell* 17(1):98–110.
63. Zhou J, Patel TR, Fu M, Bertram JP, Saltzman WM (2012) Octa-functional PLGA nanoparticles for targeted and efficient siRNA delivery to tumors. *Biomaterials* 33(2):583–591.
64. Nance EA, et al. (2012) A dense poly(ethylene glycol) coating improves penetration of large polymeric nanoparticles within brain tissue. *Sci Transl Med* 4(149):149ra119.